FRINGING EFFECTS IN THE OPERATION OF HARMONIC BACKING POTENTIAL KELVIN PROBES

G. CHIRITOI, F. A. POPESCU*

Institute of Space Science – INFLPR Subsidiary, Atomistilor Str., No. 409, Magurele, Ilfov County, Romania
* *E-mail*: fapopescu@spacescience.ro

Received April 18, 2024

Abstract. In this paper we present the effects of fringing on the measurement of the tip-sample capacitance for Kelvin probes driven by a harmonic backing potential. Moreover, we show that in this case it is still possible to obtain good estimations of operational parameters that allow for the fully controlled operation of harmonically driven Kelvin probes.

Key words: fringing effects, Kelvin probe, backing potentials.

DOI: https://doi.org/10.59277/RomJPhys.2024.69.910

1. INTRODUCTION

The Kelvin probe method [1] is among the simplest methods for characterizing the local state of a sample surface. Indeed, by measuring the current through a variable separation capacitor formed between a tip and the sample, Kelvin Probes (KPs) can determine the local contact potential difference (V_{CPD}) between the materials of the tip and of the sample, and repeated measurements in the time domain can offer information on the dynamics of the sample's surface (*e.g.* caused by contamination in air, desorption in vacuum, etc.).

From the functional viewpoint, commercially available KP instruments operate with a switching backing potential (square wave actually) applied to the tip electrode, and while this approach for the tip biasing has proven efficient, it does have certain performance limiting drawbacks. The most significant of the latter are the time delays associated with the decay of the transients occurring in the front-end electronics due to the switching of the backing potential between the high and low levels of the square wave which effectively reduce the time resolution of the V_{CPD} measurements to the range of 50–100 ms or more depending on the user choice of operational settings, and the difficulty in directly and independently monitor and control both the tip-sample separation and the tip oscillation amplitude (henceforth referred to as d_0 and respectively d_1, see Fig. 1 in the next section) about conveniently chosen setpoints.

A rather obvious alternative to the switching backing potential KP (SBPKP) is the harmonic backing potential KP (HBPKP) configuration, in which the tip biasing square-wave backing potential waveform is replaced by a sinusoidal (harmonic)

waveform [2]. The use of the latter type of tip biasing waveforms solves in a trivial way the FEE transient delay issue, increasing the time resolution of the V_{CPD} measurements to essentially the time resolution of the instrument's data acquisition system, and furthermore, it allows by using Fourier techniques for the tip current [2, 3] to independently measure and hence control the tip-sample separation d_0 and the tip oscillation amplitude d_1.

The operation of an HBPSKP instrument relies heavily on the choice of operational model used to describe the tip-sample capacitance, and commonly, this operational model is that of a thin parallel plane capacitor [1, 2, 3] whose capacitance is given by the standard expression:

$$C = \frac{\varepsilon_0 S}{d(t)} \tag{1}$$

with $\varepsilon_0 = 8.854 \times 10^{-12}$ F/m the electric permittivity of free space, S is the area of the tip electrode (usually modeled as a thin disk of radius R) and $d(t)$ the variable tip-sample spacing. This model of the capacitance is reasonably accurate for small electrodes separations $d(t) << R$ where fringing effects can be neglected. However, for typical KP instruments the size of the tip electrode is of the order of $R \approx 1$–5 mm and they operate at tip-sample separations of the order of $d_0 \approx 10$–50 μm which is a regime where fringing effects become non-negligible.

Under these circumstances, in the present paper we develop an operational model for HBPSKP instruments that accounts for the effects of fringing on the tip-sample capacitance, and we investigate the influence of these effects on the tip current and on the measurement of V_{CPD} and of the tip-sample separation d_0 and the tip oscillation amplitude d_1.

The paper is organized as follows. In Section 2 we present the HBPKP no-fringing operation model as well as the fringing operational models that account for fringing effects on the tip-sample capacitance, and provide the methodology for estimating V_{CPD}, d_0 and d_1 from the Fourier representation of this model. In Section 3 we discuss the influence of fringing effects on the tip-sample capacity and current as well as on the estimation of V_{CPD} and of the HBPKP operational parameters d_0, γ and d_1, and in Section 4 we conclude the paper with a summary of our results and their implications on the operation of HBPKP instruments.

2. HBPKP OPERATIONAL MODEL WITH FRINGING EFFECTS

Consider the KP configuration depicted in Fig. 1, where the tip electrode is assumed to be a thin disk of radius R and the sample an infinite conducting plane. As mentioned in the previous section, for $d(t) << R$, eq. (1) is a reasonable approximation for capacity when fringing effects can be neglected, which in turn –

by virtue of the image theorem in electrostatics – allows one to describe tip-sample capacity in the disk-plane measurement configuration as:

$$C(t) = \frac{2\varepsilon_0 S}{d(t)} \tag{2}$$

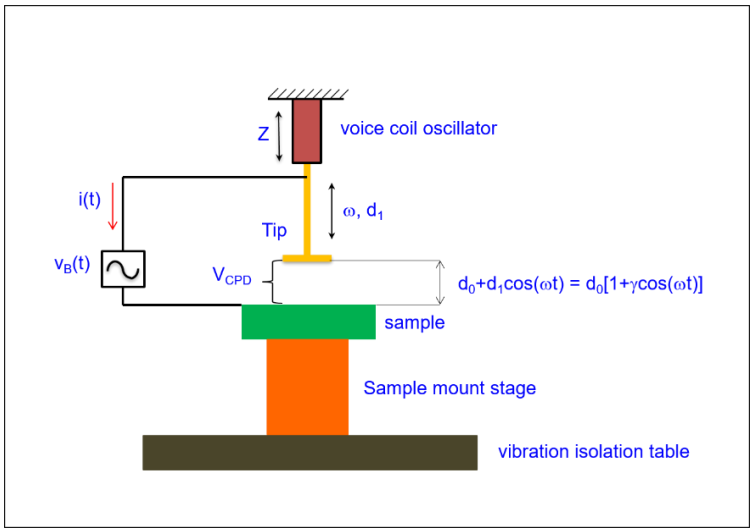

Fig. 1 – Standard HBPKP operational configuration with a disk-shaped tip.

Under these circumstances, for a harmonic backing potential $v_B(t)$ and respectively a tip-sample separation $d(t)$ given by:

$$v_B(t) = V_{B0}\sin(\omega_B t) \tag{3}$$

$$d(t) = d_0 + d_1\cos(\omega_C t) = d_0[1+\gamma\cos(\omega t)] \tag{4}$$

where V_{B0} is the amplitude of the harmonic backing potential, $\omega_B = 2\pi f_B$ and $\omega_C = = 2\pi f_C$ the angular frequencies associated with the backing potential oscillation frequency f_B and respectively the tip oscillation frequency f_C, d_0 the (average) tip-sample separation, d_1 the tip oscillation amplitude and $\gamma = d_1/d_0$ the tip modulation index, the tip-sample capacitance will have the explicit expression:

$$C(t) = \frac{2C_0}{[1+\gamma\cos(\omega_C t)]} \tag{5}$$

the charge on the tip will be:

$$Q(t) = [V_{B0}\sin(\omega_B t) - V_{CPD}]C(t) \tag{6}$$

and the tip-sample current will have the expressions [2]:

$$i(t) = \frac{\mathrm{d}Q(t)}{\mathrm{d}t} = [V_{\mathrm{B0}}\sin(\omega_{\mathrm{B}}t) - V_{\mathrm{CPD}}]\frac{\mathrm{d}C(t)}{\mathrm{d}t} + \omega_{\mathrm{B}}C(t)V_{\mathrm{B0}}\cos(\omega_{\mathrm{B}}t) = \\ = 2\gamma\omega_{\mathrm{C}}C_0[V_{\mathrm{B0}}\sin(\omega_{\mathrm{B}}t) - V_{\mathrm{CPD}}]\frac{\sin(\omega_{\mathrm{C}}t)}{[1+\gamma\cos(\omega_{\mathrm{C}}t)]^2} + \frac{2\omega_{\mathrm{B}}C_0V_{\mathrm{B0}}\cos(\omega_{\mathrm{B}}t)}{[1+\gamma\cos(\omega_{\mathrm{C}}t)]} \quad (7)$$

with $C_0 = \varepsilon_0\pi R^2/d_0$ being half of the tip-sample capacitance corresponding to the average value of $d(t)$. The tip-sample current admits a Fourier series representation of the form:

$$i(t) = BV_{\mathrm{B0}}\cos(\omega_{\mathrm{B}}t) + ABV_{\mathrm{B0}}\cos(2\omega_{\mathrm{B}}t) - 3ABV_{\mathrm{CPD}}\sin(3\omega_{\mathrm{B}}t) - \\ - 2ABV_{\mathrm{B0}}\cos(4\omega_{\mathrm{B}}t) - \frac{5}{2}A^2BV_{\mathrm{B0}}\cos(5\omega_{\mathrm{B}}t) + 6A^2BV_{\mathrm{CPD}}\sin(6\omega_{\mathrm{B}}t) + \\ + \frac{7}{2}A^2BV_{\mathrm{B0}}\cos(7\omega_Bt) + 4A^3BV_{\mathrm{B0}}\cos(8\omega_Bt) - 9A^3BV_{\mathrm{CPD}}\sin(9\omega_Bt) - \\ -5A^3BV_{\mathrm{B0}}\cos(10\omega_Bt) - \frac{11}{2}A^4BV_{\mathrm{B0}}\cos(11\omega_Bt) + \\ +12A^4BV_{\mathrm{CPD}}\sin(12\omega_{\mathrm{B}}t) + \frac{13}{2}A^4BV_{\mathrm{B0}}\cos(13\omega_{\mathrm{B}}t) + \ldots \quad (8)$$

where in eq. (6) we have assumed for practical reasons that $\omega_{\mathrm{C}} = k\omega_{\mathrm{B}}$ with $k = 3$, and we have used the notations:

$$A = \frac{\gamma}{1+\sqrt{1-\gamma^2}} \quad (9)$$

$$B = \frac{4\omega_{\mathrm{B}}C_0}{\sqrt{1-\gamma^2}}. \quad (10)$$

To develop an HBPKP operational model that includes fringing, from the practical viewpoint one must replace in eqs. (4) and (5) the parallel-plate capacitance model described by eq. (2) with a more appropriate capacitance model that includes the effects of fringe electrical fields arising at the edges of the electrode forming the tip-sample capacitor, and eventually also the effects of the thickness of the said electrode. In practice however, as the sample is usually much larger in size than the tip electrode, and since the tip electrode can be considered to the first order as a thin electrode, the issue of finding an appropriate model for the tip-sample capacitance reduces to the problem of calculating the capacitance of a system consisting of a disk of radius R

separated by a distance *d* from an infinite grounded conducting plane. This problem, which is equivalent by the theorem of images to the calculation of the capacitance of a parallel-plate capacitor with two disk electrodes of radius *R* and separated by a distance 2*d*, is one of the classical problems in electrostatics. In this context, it has received intense attention at various times in the last century in relation to both theoretical interest in the development of methods and tools for solving general electrostatic problems as well as in relation to advances in technology (*e.g.* the development of electrostatic lenses for particle accelerators, the development of mechanical sensor and actuators, the miniaturization of such sensors and actuators in the context of MEMS and NEMS technology advances, etc.). As such, a rather extensive survey of the published literature on the topic has shown that the most common model of the thin disk-grounded plane capacitance is described by the expression:

$$C(t) = \frac{2\pi\varepsilon_0 R^2}{d(t)}\left\{1 + \frac{d(t)}{\pi R}\ln\left[\frac{\alpha R}{d(t)}\right]\right\} \tag{11}$$

where $\alpha = 16\pi/e$ describes the Kirchhoff approximation [4], $\alpha = 64/e$ describes the Ignatowski approximation [5] and $\alpha = 2\pi e$ describes the Cook approximation [6], with "e" is the basis of the natural logarithm function and the rest of the symbols defined in earlier in this section. The derivation of these approximations is beyond the scope of this paper, and for more details, the reader is referred to the excellent reviews in [7] and [8].

Under these circumstances, and in a manner similar to the one used earlier in this section, the tip-sample capacitance will be given by:

$$C(t) = \frac{2C_0}{[1 + \gamma\cos(\omega_C t)]} + D\ln\left(\frac{F}{d_0}\right) - D\ln[1 + \gamma\cos(\omega_C t)] \tag{12}$$

and the tip-sample current will have the expression:

$$\begin{aligned} i(t) = \frac{\mathrm{d}Q(t)}{\mathrm{d}t} &= [V_{B0}\sin(\omega_B t) - V_{CPD}]\frac{\mathrm{d}C(t)}{\mathrm{d}t} + \omega_B C(t) V_{B0}\cos(\omega_B t) = \\ &= \frac{2\gamma\omega_C V_{B0} C_0 \sin(\omega_C t)\sin(\omega_B t)}{[1 + \gamma\cos(\omega_C t)]^2} - \frac{2\gamma\omega_C V_{CPD} C_0 \sin(\omega_C t)}{[1 + \gamma\cos(\omega_C t)]^2} + \\ &+ \frac{\gamma\omega_C V_{B0} D\sin(\omega_C t)\sin(\omega_B t)}{1 + \gamma\cos(\omega_C t)} - \frac{\gamma\omega_C V_{CPD} D\sin(\omega_C t)}{1 + \gamma\cos(\omega_C t)} + \\ &+ \frac{2\omega_B V_{B0} C_0 \cos(\omega_B t)}{1 + \gamma\cos(\omega_C t)} - \omega_B V_{B0} D\cos(\omega_B t)\ln[1 + \gamma\cos(\omega_C t)] + \\ &+ \omega_B V_{B0} D\cos(\omega_B t)\ln\left(\frac{F}{d_0}\right) \end{aligned} \tag{13}$$

where besides the notation introduced earlier, we have also introduced:

$$D = 2\varepsilon_0 R$$
$$F = \alpha R \tag{14}$$

Similar to the previous case, the tip-sample current admits a Fourier series representation, which for $\omega_C = k\omega_B$ with $k = 3$ reads:

$$\begin{aligned} i(t) = {} & \left\{ AV_{B0} + \omega_B V_{B0} D \ln\left(\frac{F}{d_0}\right) - \omega_B V_{B0} D \ln\left[\frac{1}{2}\left(1+\sqrt{1-\gamma^2}\right)\right]\right\}\cos(\omega_B t) + \\ & + V_{B0} A(2\omega_B D - 2B)\cos(2\omega_B t) + V_{CPD}(6\omega_B D + 3B)\sin(3\omega_B t) + \\ & + V_{B0} A(B - 4\omega_B D)\cos(4\omega_B t) + V_{B0} A^2\left(\frac{7}{2}B - \frac{5}{2}\omega_B D\right)\cos(5\omega_B t) - \\ & - V_{CPD} A^2(6B + 6\omega_B D)\sin(6\omega_B t) + V_{B0} A^2\left(\frac{7}{2}\omega_B D - \frac{5}{2}B\right)\cos(7\omega_B t) - \\ & - V_{B0} A^3\left(5B + \frac{10}{3}\omega_B D\right)\cos(8\omega_B t) + V_{CPD} A^3(9B + 6\omega_B D)\sin(9\omega_B t) - \\ & - V_{B0} A^3\left(5B + \frac{10}{3}\omega_B D\right)\cos(10\omega_B t) + V_{B0} A^4\left(\frac{13}{2}B - \frac{11}{4}\omega_B D\right)\cos(11\omega_B t) - \\ & - V_{CPD} A^4(12B + 6\omega_B D)\sin(12\omega_B t) + V_{B0} A^4\left(\frac{13}{4}\omega_B D - \frac{11}{2}B\right)\cos(13\omega_B t) + \\ & + \cdots \end{aligned} \tag{15}$$

3. EFFECTS OF FRINGING ON THE HBPKP CURRENT MEASUREMENT

Consider now a typical HBPKP experimental configuration, with R = 2.5 cm, d_0 = 10 μm, d_1 = 9 μm (γ = 0.9), V_{B0} = 1 V, V_{CPD} = 0.4 V, f_B = 2 kHz, f_C = 6 kHz (k = 3). Under these circumstances, using eqs. (5) and (18), the tip-sample capacitance with and without fringing effects over one period T_B = 0.5 ms (=1/f_C) is illustrated in Fig. 2. As can be seen from this figure, the value of the capacitance with no fringing varies from ~ 18.3 pF for maximum tip-sample separation (d = 19 μm) to ~ 348 pF for minimum tip-sample separation (d = 1 μm), and the fringing models follow very closely the no-fringing model.

The relative differences of the fringing capacitances in the three models – Kirchhoff, Ignatowski and Cooke – relative to the no-fringing model described by eq. (5) are illustrated in Fig. 3. According to this figure, the largest deviation from the non-fringing capacitance is provided by the Ignatowski approximation, spanning the range from ~0.356 pF (1.944%) at maximum tip-sample separation to ~ 0.486 pF (~0.139%) at minimum tip-sample separation. Following is the Kirchhoff approximation, with deviations spanning the range from ~ 0.345 pF (~ 1.86%) to ~ 0.475 pF (~ 0.137%)

and the Cooke approximation with deviations spanning the range from ~ 0.341 pF (~ 1.866%) to ~ 0.471 pF (~ 0.136%).

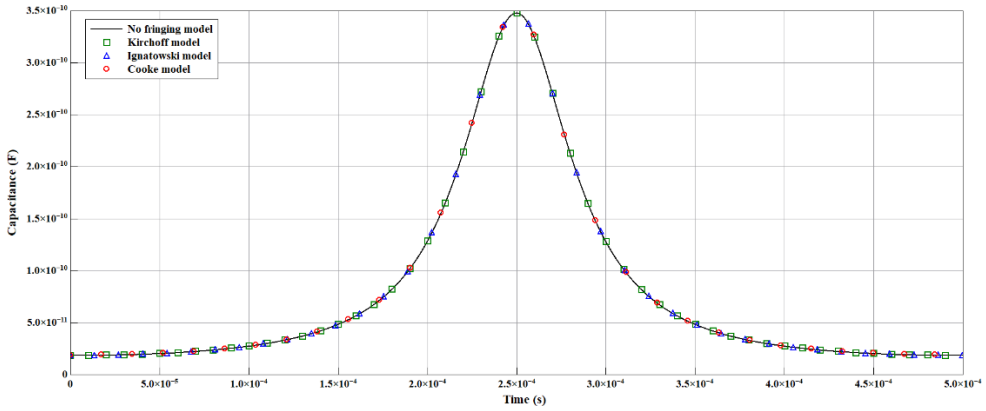

Fig. 2 – Tip-sample capacitance with no fringing (solid black line) and with fringing (Kirchhoff model – green square, Ignatowski model – blue triangle and Cooke model – red circle).

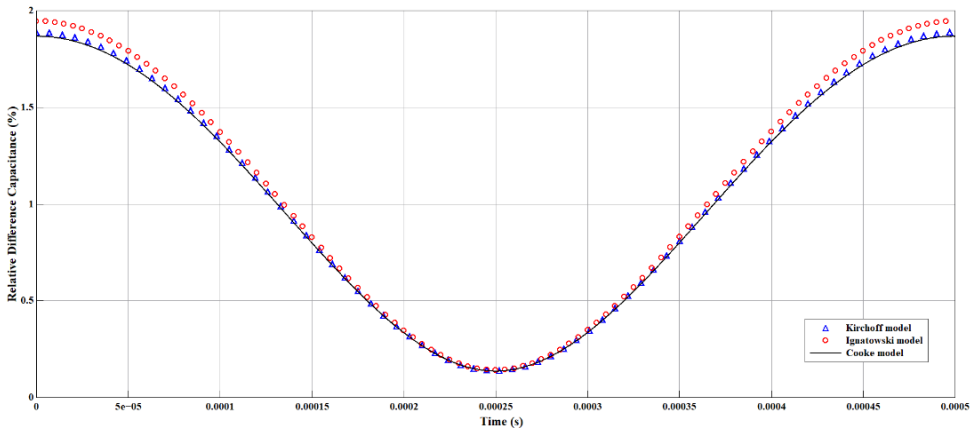

Fig. 3 – Relative diffenrences of the capacitances with fringing (Kirchhoff model – solid black line, Ignatowski model – red circle, Cooke model – blue triangle) with respect to the no-fringing capacitance.

A similar analysis can be performed for the tip-sample current as given by eqs. (7) and (16). For the same experimental configuration, the currents associated with the no-fringing and fringing current models are illustrated over a period T_B = 0.5 ms (= $1/f_B$) in Fig. 4. As the figure shows, in the experimental conditions described earlier the tip-sample current has a significant spectral content, and the Kirchhoff, Ignatowski and Cooke approximations follow closely the no-fringing current described by eq. (7).

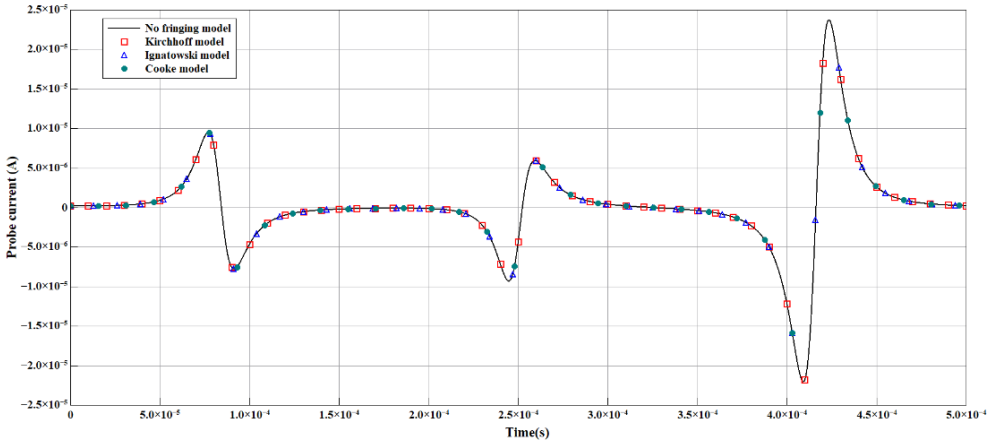

Fig. 4 – Tip-sample current in the absence of fringing (solid black line) and with fringing (Kirchhoff approximation - red square, Ignatowski approximation – blue triangle and Cooke approximation – green dot).

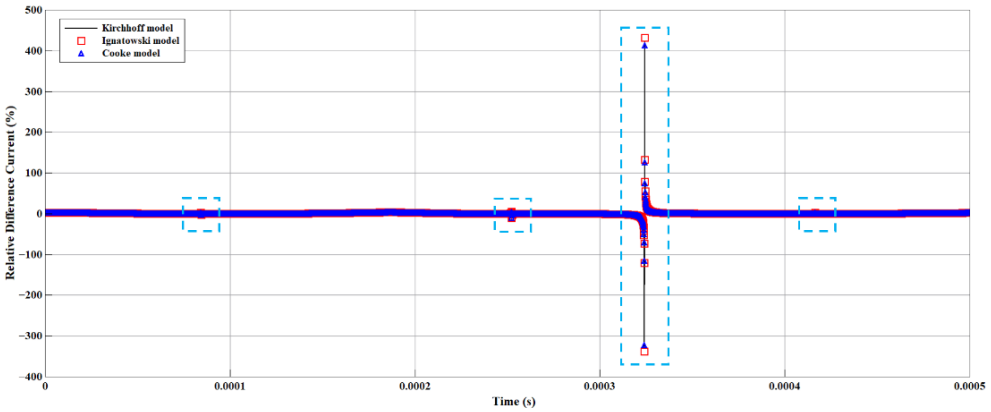

Fig. 5 – Relative differences of the tip-sample fringing currents (the Kirchhoff model – solid black line, Ignatowski model – red square, Cooke model – blue triangle) relative to the no-fringing current. Excess fringing current regions are marked by light-blue dashed squares.

The relative differences of the currents corresponding to the Kirchhoff, Ignatowski and Cooke models relative to the no-fringing model described by eq. (7) are pretty much benign, ranging from ~ 0.04% to ~ 2% over most of the sampled period. However, and by contrast to the similar capacitance data in Fig. 3, there are several regions – their number depending on the interplay of the values of the f_B and f_C frequencies and of the value of the modulation index γ – where the magnitudes of the fringing currents exceed the above range, and sometimes significantly, as illustrated in Fig. 5. As can be seen in the graph, for the experimental configuration

under consideration, there are four such regions where the fringing currents can exceed the non-fringing current from ~13% (the leftmost region) up to ~400% (second rightmost region).

As the HBPKP instrument relies on model-based numerical processing of the tip-sample current information for measuring the V_{CPD} and controlling the instrument operation (measuring the operational parameters d_0 and d_1 or alternatively d_0 and γ), it is important to investigate the effects of fringing on the estimation accuracy of these parameters. This can be achieved by assuming a HBPKP instrument controlled by the no-fringing model described by eqs. (5)–(10) – the simplest operational model from both the physics and numerical implementation viewpoint – that operates on datasets generated with the fringing models described by eqs. (11)–(15). Furthermore, in order to have a realistic evaluation of these effects on the instrument operation, we will also assume a minimal FEE current measurement system consisting of an ideal op-amp transimpedance amplifier (TIA) stage – a common FEE system for KP instruments, be they independent or part of a more elaborate SPM system – with a feedback resistor R_f = 1 MΩ as the one in Fig. 6 below.

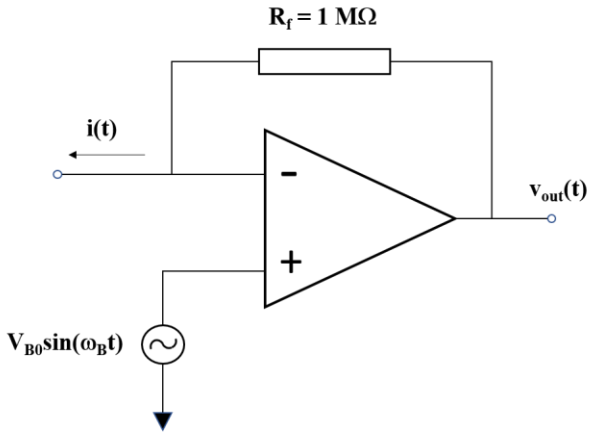

Fig. 6 – Ideal op-amp TIA stage for the HBPKP instrument.

With the TIA stage in Fig. 6, the measurement signal will be given by:

$$v_{\mathrm{out}}(t) = V_{\mathrm{B0}} \sin(\omega_{\mathrm{B}} t) + i(t) R_{\mathrm{f}} \tag{16}$$

where $v_{out}(t)$ is the output signal of the TIA stage that carries all the information about the tip-sample current given by eqs. (7) or (8) in the no-fringing case and by eqs. (13) or (15) in the fringing case.

As the HBPKP system is operated and controlled by a no-fringing model, the tip-sample current will be described by eq. (7) and will have a Fourier series

representation given by eq. (8). Under these circumstances, the Fourier representation of TIA output signal will be:

$$\begin{aligned} v_{\text{out}}(t) = {} & V_{\text{B0}}\sin(\omega_{\text{B}}t) + R_{\text{f}}BV_{\text{B0}}\cos(\omega_{\text{B}}t) + R_{\text{f}}ABV_{\text{B0}}\cos(2\omega_{\text{B}}t) - \\ & -3R_{\text{f}}ABV_{\text{CPD}}\sin(3\omega_{\text{B}}t) - 2R_{\text{f}}ABV_{\text{B0}}\cos(4\omega_{\text{B}}t) - \\ & -\frac{5}{2}R_{\text{f}}A^2BV_{\text{B0}}\cos(5\omega_{\text{B}}t) + 6R_{\text{f}}A^2BV_{\text{CPD}}\sin(6\omega_{\text{B}}t) + \\ & +\frac{7}{2}R_{\text{f}}A^2BV_{\text{B0}}\cos(7\omega_{\text{B}}t) + 4R_{\text{f}}\cos(11\omega_{\text{B}}t) + \\ & +12R_{\text{f}}A^4BV_{\text{CPD}}\sin(12\omega_{\text{B}}t) + \frac{13}{2}R_{\text{f}}A^4BV_{\text{B0}}\cos(13\omega_{\text{B}}t) + \ldots \equiv \\ & \equiv \sum_{n=1}^{\infty} i_{\text{Sn}}\sin(n\omega_{\text{B}}t) + \sum_{n=1}^{\infty} i_{\text{Cn}}\cos(n\omega_{\text{B}}t) \end{aligned} \tag{17}$$

with i_{Sn}, i_{Cn} the generic coefficients of the TIA output signal Fourier representation that can be calculated according to the relations:

$$i_{\text{Sn}} = \frac{\omega_{\text{B}}}{\pi} \sum_{\text{datapoints/period}} i_{\text{r}}\sin(\text{n}\omega_{\text{B}}t_{\text{r}}) \tag{18}$$

$$i_{\text{Cn}} = \frac{\omega_{\text{B}}}{\pi} \sum_{\text{datapoints/period}} i_{\text{r}}\cos(\text{n}\omega_{\text{B}}t_{\text{r}}) \tag{19}$$

Using the Fourier representation of the TIA output signal in eq. (17), V_{CPD} and the operational parameters of the HBPP instrument can be readily estimated as:

$$\begin{aligned} V_{\text{CPD}} &= -\frac{1}{3}\alpha_{\text{SC32}}V_{\text{B0}} \\ \gamma &= -\frac{20\,\alpha_{\text{CC52}}}{25 + 4\,\alpha_{\text{CC52}}^2} \\ d_0 &= -\frac{8}{5}(\omega_{\text{B}}R_{\text{f}}\varepsilon_0\pi R^2)\left(\frac{\alpha_{\text{CC52}}}{\alpha_{\text{CS21}}}\right)\left(\frac{25 + 4\,\alpha_{\text{CC52}}^2}{25 - 4\,\alpha_{\text{CC52}}^2}\right) \\ d_1 &= \gamma d_0 \end{aligned} \tag{20}$$

where in eq. (20) we have used for ratios of Fourier amplitudes of the TIA output signal the notations:

$$\alpha_{SC32} = \frac{i_{S3}}{i_{C2}}$$
$$\alpha_{CC52} = \frac{i_{C5}}{i_{C2}} \qquad (21)$$
$$\alpha_{CS21} = \frac{i_{C2}}{i_{S1}}$$

With these considerations in place, and using the experimental configuration described earlier in this section, we have simulated the output of the TIA in both the no-fringing and fringing cases, and have used eqs. (18)–(21) to estimate V_{CPD} and the operational parameters γ and d_0 as a function of the input value of γ used to generate the associated datasets. The results are presented in Fig. 7 – Fig. 9.

Fig. 7 illustrates the (relative) signed estimation error of the contact potential difference V_{CPD} with respect to the input value of V_{CPD} = 0.4 V used in simulating the TIA output.

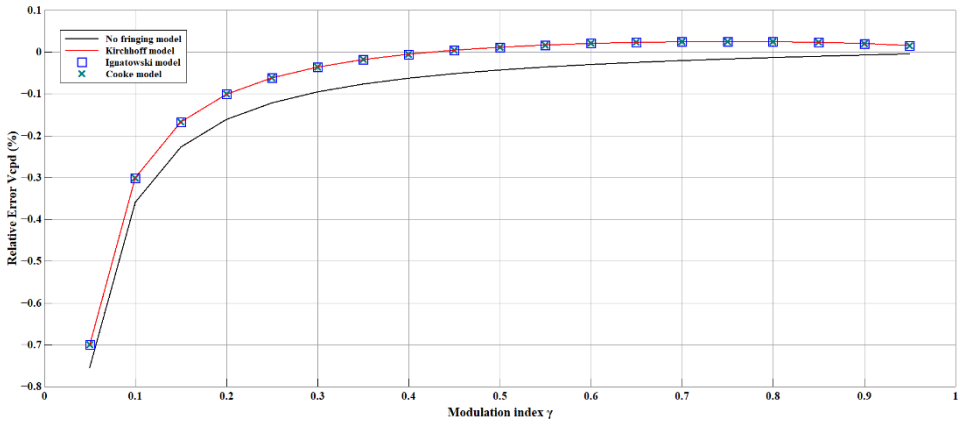

Fig. 7 – Relative error for V_{CPD} estimated from the no-fringing (solid black line) and fringing models datasets (Kirchhoff model – red solid line, Ignatowski – blue square, Cooke – green diagonal cross) and the value of V_{CPD} that was used as input for the generation of these datasets.

Besides the data corresponding to the Kirchhoff, Ignatowski and Cooke fringing models, we have also included, for reasons of completeness, the data for the standard no-fringing model described by eq. (5). As can be seen from this figure, the estimation precision, irrespective of the model used in simulating the data, improves

with increasing value of the modulation index γ. Furthermore, even for very small values of γ (*e.g.* γ = 0.05 – which in practice would be an unreasonably small value for γ) the estimation error does not exceed 0.7%, which is more than reasonable in practice. For values of γ that are common in practice (*e.g.* γ ≥ 0.5), the estimation error – once more, irrespective of the model used in simulating the data – drops to below 0.1%. It is interesting to note that while in the no-fringing case, the HBPKP no-fringing operational model consistently underestimates V_{CPD}, for the fringing cases V_{CPD} is underestimated up to γ ≅ 0.4 and overestimated above this value. Even more interesting is the fact that while in the no-fringing case the estimation error improves monotonically, in all the fringing cases, the overestimation reaches a maximum and then starts decreasing towards large values of γ. All of these suggest that in practice there may be an optimum value for the modulation index γ that could minimize the error in estimating the contact potential difference V_{CPD}.

Fig. 8 illustrates the (relative) signed estimation error of modulation index γ with respect to the input value of γ used in simulating the TIA output. As it can be seen from this figure, all data models consistently underestimate the value of γ on the entire range under consideration, with the estimation error improving monotonically with increasing value of γ. For small values of γ, the estimation error of γ is ~ 13% (still not too bad in practice), while for values of γ that are common in practice (*e.g.* γ ≥ 0.5), the estimation error drops down to below 0.03%.

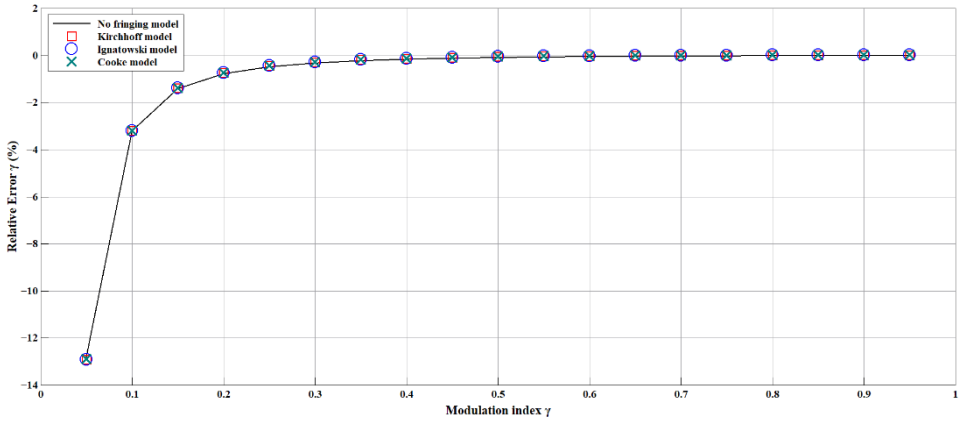

Fig. 8 – Relative error for the modulation index γ estimated from the no-fringing (solid black line) and fringing models datasets (Kirchhoff model – red square, Ignatowski – blue circle, Cooke – green diagonal cross) and the value of γ used as input for the generation of these datasets.

Fig. 9 illustrates the (relative) signed estimation error of tip-sample separation d_0 with respect to the input value of d_0 = 10 μm used in simulating the TIA output. Much like in the case of the modulation index γ, irrespective of the model used for

the simulation of data, d_0 is consistently underestimated and its estimation error improves monotonically with increasing γ from ~ 14% for small values of γ to below 0.04% for commonly used in practice values of γ (*e.g.* $\gamma \geq 0.5$). In particular, this means that in the latter case, the tip-sample separation d_0 can be estimated with an accuracy of ~ 40 nm, which in turn means that the operational model under discussion well suited for the implementation of a feedback control system to keep the tip-sample distance constant during data acquisition (for static instruments) and/or scanning (for scanning instruments).

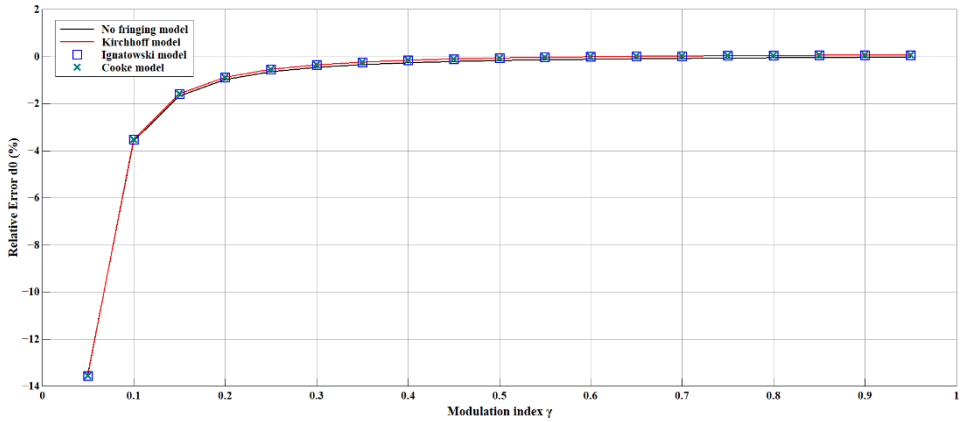

Fig. 9 – Relative error for d_0 estimated from the no-fringing (solid black line) and fringing models datasets (Kirchhoff model – red square, Ignatowski – blue square, Cooke – green diagonal cross) and the value of d_0 used as input for the generation of these datasets.

Equally important also is the fact that since the oscillation amplitude is $d_1 = \gamma d_0$, the information in the last two figures allow one to state that for values of γ that are common in practice (*e.g.* $\gamma \geq 0.5$), the oscillation amplitude d_1 can be estimated with an error better than ~ 0.05% (this would mean an error better than 25 nm for $d_1 = 5$ μm in the case where $\gamma = 0.5$ and $d_0 = 10$ μm). Once more, this means that the operational model under consideration for the HBPKP is very well suited for the implementation of a feedback control system (separate HW-wise from the one mentioned previously) to keep the tip oscillation amplitude constant during data acquisition and scanning for both static and scanning HBPKP instrument, and which together with the feedback control system for the tip-sample separation d_0 would allow for the complete control of the HBPKP instrument during its operation.

4. SUMMARY AND CONCLUSIONS

To summarize the results presented in the previous sections, to investigate the effects of fringing between the tip of an HBPKP instrument and the sample, one can

use three fringing models, namely the Kirchhoff model, the Ignatowski model and respectively the Cooke model. Referring to the tip-sample capacity and to the tip-sample current, all these fringing models are described essentially by the same functional relation, namely eq. (11) for the tip-sample capacity and eq. (13) for the tip-sample current, and the difference only arise in the choice of certain constants in these equations as described in Section 2. The investigation of the effects of fringing on the tip-sample capacitance under typical experimental conditions has revealed that fringing leads to a maximum increase of ~ 1.9% with respect to the no-fringing capacitance model, irrespective of the choice of the fringing model. Similarly, for the tip-sample current, the effects of fringing lead to an average increase of ~ 2% of the capacitance with respect to the no-fringing capacitance, although there are regions – over the course of one oscillation period of the backing potential – where the fringing current can exceed by ~ 400% the non-fringing current.

We have also investigated the effects of fringing on the estimation accuracy of the contact potential difference V_{CPD} and of the instrument's operational parameters d_0 – the tip-sample separation, γ – the tip amplitude modulation index and d_1 – the tip oscillation amplitude, under the circumstances where an HBPKP instrument is operated under typical experimental conditions and controlled by a no-fringing operational model. In this case, and for $\gamma \geq 0.5$, the contact potential difference can be estimated from experimental data with an error below 0.1 percent, while the operational parameters d_0, γ and d_1 can be estimated with errors below 0.03%, 0.03% and respectively 0.04%.

All these results suggest that in the presence of fringing, an HBPKP instrument operating under typical experimental conditions and with a no-fringing operational model can allow for the full and separate active control of its operational parameters (d_0, γ) or (d_0, d_1) during the data acquisition and/or scanning process in order to ensure the consistency of the V_{CPD} measurement.

Acknowledgements. This work was supported by a grant of the Romanian Ministry of Education and Research, CCCDI – UEFISCDI, project number PN-III-P2-2.1-PED-2019-2797, within PNCDI III.

REFERENCES

1. I. D. Baikie, *Old Principles… New Techniques: A Novel UHV Kelvin Probe and its Application in the Study of Semiconductor Surfaces*, Enschede, The Netherlands, 1988.
2. G. Chiritoi *et al.*, Rom. Rep. Phys. **71**, 801 (2019).
3. E. M. Popescu, Class. Quant. Grav. **28**, 225005 (2011).
4. W. Ignatowski, Akad. Nauk SSSR Mat. Inst Trudy **2**(3), 1 (1932).
5. J. C. Cooke, Z. Angew. Math. Mech **38**, 149 (158).
6. Ian N. Sneddon, *Mixed boundary value problems in potential theory*, North-Holland Publishing Company – Amsterdam, 1966.
7. V. Hutson, Proc. Camb. Phil. Soc. **59**, 211 (1963).
8. G. J. Sloggett *et al.*, J. Phys. A Math. Gen. **19**, 2725 (1986).